Characterization of Bacterial Nanocellulose - Graphite Nanoplatelets Composite Films

Bili Darnanto Susilo[1], Heru Suryanto[2, 3,*], Aminnudin[2]

[1]*Master Program of Mechanical Engineering, Universitas Negeri Malang, Jl. Semarang 5, Malang 65145, Indonesia*
[2]*Center of Excellence for Cellulose Composite (CECCom), Department of Mechanical Engineering, Faculty of Engineering, Universitas Negeri Malang, Jl. Semarang 5, Malang 65145, Indonesia*
[3]*Centre of Advanced Material for Renewable Energy (CAMRY), Universitas Negeri Malang, Jl. Semarang 5, Malang 65145, Indonesia*
**Corresponding author: heru.suryanto.ft@um.ac.id*

ABSTRACT

Bacterial cellulose (BC) was synthesized from pineapple peel extract media with addition of fermentation agent bacteria Acetobacter xylinum. BC was disintegrated from the pellicle into bacterial nanocellulose (BNC) by using a high-pressure homogenizer (hph) machine, which has a three-dimensional woven nanofibrous network. The synthesis of composite films started when BNC, graphite nanoplatelets, and cetyltrimethylammonium bromide (CTAB) were homogenized using an ultrasonic homogenizer then baked on a glass mold at a temperature of 80 degrees Celcius for 14h. A scanning electron microscope (SEM) was used to analyze its morphology. X-Ray diffraction spectra were used to analyze the composite films structure. The functional groups of the composite films were analyzed using the FTIR spectrum. SEM micrograph shows that GNP was evenly distributed into BNC matrix after CTAB addition. GNPs are shown as flat and smooth flakes with sharp corners. Some peak corresponds O-H, C-H, C≡C, and CH_3 stretching was identified by using FTIR spectroscopy at wavenumber 3379, 2893, 2135, and 1340 cm^{-1}, respectively. XRD analysis shows that Crystalline Index (C.I) of BNC increases after 2.5 wt% addition of GNP. The presence of CTAB decreases C.I value of composite films. BNC/GNP composite films have the best mechanical properties with Young's modulus about 77.01 ± 8.564.

Keywords: *Bacterial nanocellulose, CTAB, FTIR, graphite nanoplatelet, morphology, XRD*

I. Introduction

Bacterial cellulose (BC) is one type of cellulose available in this world. BC seems like a hydrogel with three-dimensional tangled network of white cellulose nanofiber [1] linked by hydrogen bond [2]. Several applications of BC have been developed, the main ones being bioengineering, cosmetics, pharmaceutical, and biomedical. BC is widely known as natural polymers [3]. BC synthesized by gram-negative bacteria. The most common bacteria used in BC synthesis were *Pseudomonas aeruginosa* or *Acetobacter xylinum* [4-5]. BC is naturally synthesized from the bottom-up process by those bacteria [6], which beneficial physical properties of the resulted cellulose [7]. The extract of pineapple peel waste is used as the medium of bacterial fermentation [8]. The interesting properties of BC are chemical and thermal stability, biodegradable, mechanical strength, hydrophilicity and high crystallinity [9]. BC is the only kind of cellulose with the highest cellulose content compared to other natural cellulose, almost 100% [4].

DOI: 10.17977/um016v5i22021p145

Bacterial nanocellulose (BNC) is BC that has been disintegrated using a high-pressure homogenizer, resulting in nanosized cellulose, approximately 35-55 nm [10]. BNC was used for basic material in carbon nanofibers (CNF) manufacture. Previous supercapacitors and alkali metal batteries have used this CNF as the electrode materials [1]. Several applications of BC utilization as a binder, reinforcement agent, and to form transparent film [11]. As a result, there are many possibilities for using BNC as a basic matrix material for binder agents in energy storage device manufacture like Li-ion battery electrodes [12-13].

The physical and chemical properties of nanostructured carbons could be attractive. They are specially designed with the ability in chemical resistance, strength, good thermal and electrical conductivity and high surface area. Several previous studies have used nano carbons, hydrogen storage, nanocomposites, and catalysts for energy generation and storage. Graphite nanoplatelets (GNP) are a form of nanocarbon [14]. It is composed of graphene sheets in the form of 2D nano-sized carbon material [15]. Several properties of composite films that have been studied and proven that are affected by the presence of GNP are thermal properties, electrical, mechanical, and electrochemical [16-19]. GNP's morphology seems in the form of flat, sharp edge pieces separated from the graphite lumps at 1000 °C. These pieces have a thickness of 10-100 nm [17]. Several studies have explored the potential of GNP for composite formation purposes [21-26].

Surfactants are molecules that are both hydrophilic and hydrophobic in the same molecule. The type of surfactant was used in this work, namely cetyltrimethylammonium bromide (CTAB). CTAB is used to dissolve GNP in aqueous solvents [15, 21, 27-28]. CTAB is included in cationic surfactants. Ammonium (N^+) group becomes the head part, which is hydrophilic, and Cetyl groups become its tail part, a hydrocarbon chain that consists of hydrophobic. The polar compound would interact with the head part of CTAB, while the non-polar compound interacts with CTAB. GNP is a non-polar compound, so to disperse into a solvent, a polar compound, surfactant like CTAB is needed.

The study of bacterial cellulose-based composite films explored in several previous studies use surfactant but does not use disintegrated and homogenized BNC. The novelty of this research is using the high-pressure homogenized BNC as matrix reinforced by GNP. This study uses GNP as a reinforcement agent of the BNC matrix to produce BNC/GNP composite film with CTAB addition. BC was synthesized using pineapple peel extract media. BNC was produced through the disintegration process and then processed with high-pressure homogenizer (hph) and filtered by a vacuum filter to remove the excess water. BNC, CTAB, and GNP were mixed into distillation water media then stirred and sonicated. The presence of GNP into BNC/GNP composites film was analyzed whether its morphology, functional groups, and crystallinity of composites were measured by SEM, FTIR spectroscopy and X-Ray Diffraction, respectively.

II. Material and Methods

A. Materials

Acetobacter xylinum bacteria supplied from Laboratorium Teknologi Terapan, Universitas Muhammadiah Malang, Indonesia. BC is synthesized in a pineapple peel extract medium. Graphite nanoplatelets were supplied from CV.Gamma Scientific Biolab, Malang.Urea, sodium hydroxide and Glucose ($C_6H_{12}O_6$) were obtained from CV.Makmur Sejati, Malang, Indonesia.

B. Synthesis of BC

Referring to previously published methods by Suryanto et al. [24], BC synthesis starts with making juice from 300 gr of pineapple peel (rotten) plus water up to a volume of 2 L. The juice was then filtered. The pineapple peel extract is boiled. After boiling, add 7.5% (w/v) glucose and 0.5% (w/v) urea. Put 1 L on a tray with more than 1 L capacity, then chilled. Once cool, add a 1% (v/v) fermentation bacterial. Incubated for 14 days. The harvested BC pellicle was then washed using water, boiled using a solution of NaOH 1% at 90^{o}C for 2 hours, and washed again until neutral.

C. Synthesis of BNC

50 grams of BC pellicle and 300 milliliters of aquades disintegrated by a high-powered blender for 1.5 min. Add more 700 mL of purified water and blend again for 2 min. The cellulose solution is homogenized with hph machine for as much as five cycles at 150 bars. Then filtered using a vacuum filter to remove excess water [25].

D. Synthesis of Composite Films BNC/GNP

BNC with mass 10 grams were diluted in 100 mL of purified water. GNP with percentage 2.5% and CTAB with percentage 0.3%, diluted in 100 mL of distilled water. A magnetic stirrer is used to stir both solutions for 45 minutes. After that, the solutions merge and sonicate for an hour using an ultrasonic homogenizer. The slurry is put on a glass mold with aluminium-paper lamination and dried in an oven at 80 degrees Celcius for 14 hours [26].

E. Morphological Studies

Morphology of the composite film's observation was conducted using SEM, with 20 kV operating voltage at Advanced Mineral and Material Laboratory, Universitas Negeri Malang, Indonesia. The composite films' dimensions were cut into 10 mm x 10 mm and then coated with 10 nm gold before observation. The composite films were observed at 10.000x magnification.

F. FTIR Analysis

FTIR analysis was conducted to analyze the functional groups. The sample is scanned with a wavenumber range of 4000 to 400 cm^{-1} with 4 cm^{-1} resolution. Composite films were cut into 10 mm x 10 mm. The machine used in this test is Shimadzu IR Prestige-21 that belong to Advanced Mineral and Material Laboratory, Universitas Negeri Malang, Indonesia.

G. X-Ray Diffraction Analysis

XRD analysis was conducted (using Pan Analytical X-Pert Pro Diffractometer) at Advanced Mineral and Material Laboratory, Universita Negeri Malang, Indonesia. The dimension of composite films was cut into 10 mm x 10 mm. Scanning steps were done at 2θ degree from 10^{o} to 90^{o}. Segal equation was used to calculate the crystallinity and crystallinity index [27].

H. Tensile Strength Test

The composite films' tensile strength was tested using the TECHNO Tensile Test machine according to the ASTM D638-V standard, and the dimension of composite films was cut to 63.5 mm overall length and 9.53 mm overall width [28]. The test was carried out at the Laboratory of Nano Materials and Advanced Materials, Mechanical Engineering, State University of Malang.

III. Results and Discussions

A. Morphology

Morphology and microstructure were very important to produce nanocomposites with specific final properties and applications. Fig. 1 (a) shows an SEM micrograph of pure BNC films. Previously studied the BNC fiber diameter about 46 nm [29]. BNC has a higher surface area than BC because the cellulose fiber had been split from its hydrogen bond into a nanofiber. The pores size on BNC matrix is different because of the random arrangement of ribbon-shaped nanofiber with different. This condition makes BNC would be easier to mix uniformly with GNP. The morphology of BNC/GNP composite films shows in Fig. 1(c). GNP tends to clump due to the van der Waals force between carbon atoms and form bundles [30]. There can be seen that GNP create many bundles and does not disperse uniformly into the BNC matrix. In this work, CTAB was used as a surfactant to separate GNP bundles individually and become stable against van der Waals attraction before mixing it with BNC. Fig. 1 (b) shows the SEM micrograph of BNC/GNP composite films with the addition CTAB as surfactant. CTAB will lower the surface tension of water solvent and lower hydrophobic properties from GNP. Therefore GNP could disperse uniformly in a water solvent. Fig. 1 (b) shows nanofiber in composite films becomes more porous after mixing GNP-CTAB solution into BNC solution with less bundle of nanofiber or GNP. This could be the surfactant also. The GNPs are shown as flat and smooth flakes with sharp corners. The sonication process also effectively incorporates the GNP into the BNC matrix. Higher GNP content in the composite film will result in a larger surface area of BNC covered by GNP. GNP was used to improve the thermal and electrical conductivity, so higher GNP content will result in better thermal and electrical conductivity [21, 34].

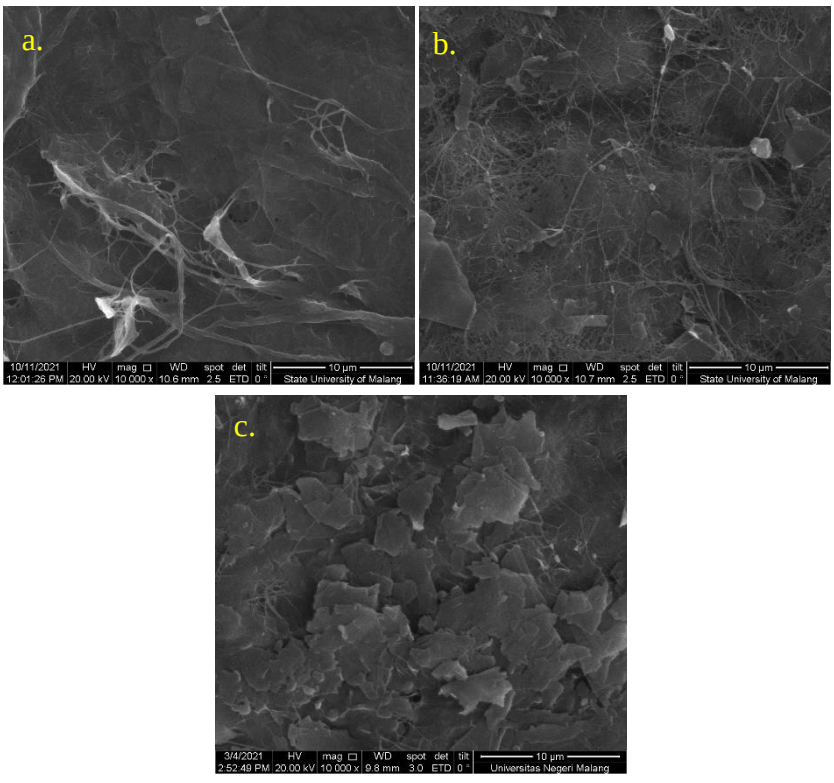

Fig. 1. SEM micrograph of composite films: a. BNC;b. BNC/GNP 2.5 wt% with CTAB addition; c. BNC/GNP 2.5 wt%.

B. FTIR Analysis

The functional groups from BNC/GNP composite films analysis were conducted based on the FTIR spectra shown in Fig. 2. The peak that corresponds to O-H stretching found at wavenumber 3379 cm^{-1}, and peak corresponds to C-H stretching peak was detected at 2893 cm^{-1} [32]. The presence of GNP in the composite films result in a lower number of O-H stretching. The peak corresponds to C≡C stretching of alkynes was identified at wavenumber 2135 cm^{-1}. After BNC was added with GNP, this peak was not appearing anymore. Peak at 1685 cm^{-1} corresponds to the O-H band from the absorbed water of the composite films. GNP's presence caused this peak to disappear because GNP made composite films temperature higher and removed the absorbed water. The peak that corresponds to CH_3 stretching was identified at wavenumber 1340 cm^{-1}, and this peak became lower after BNC was added with GNP.

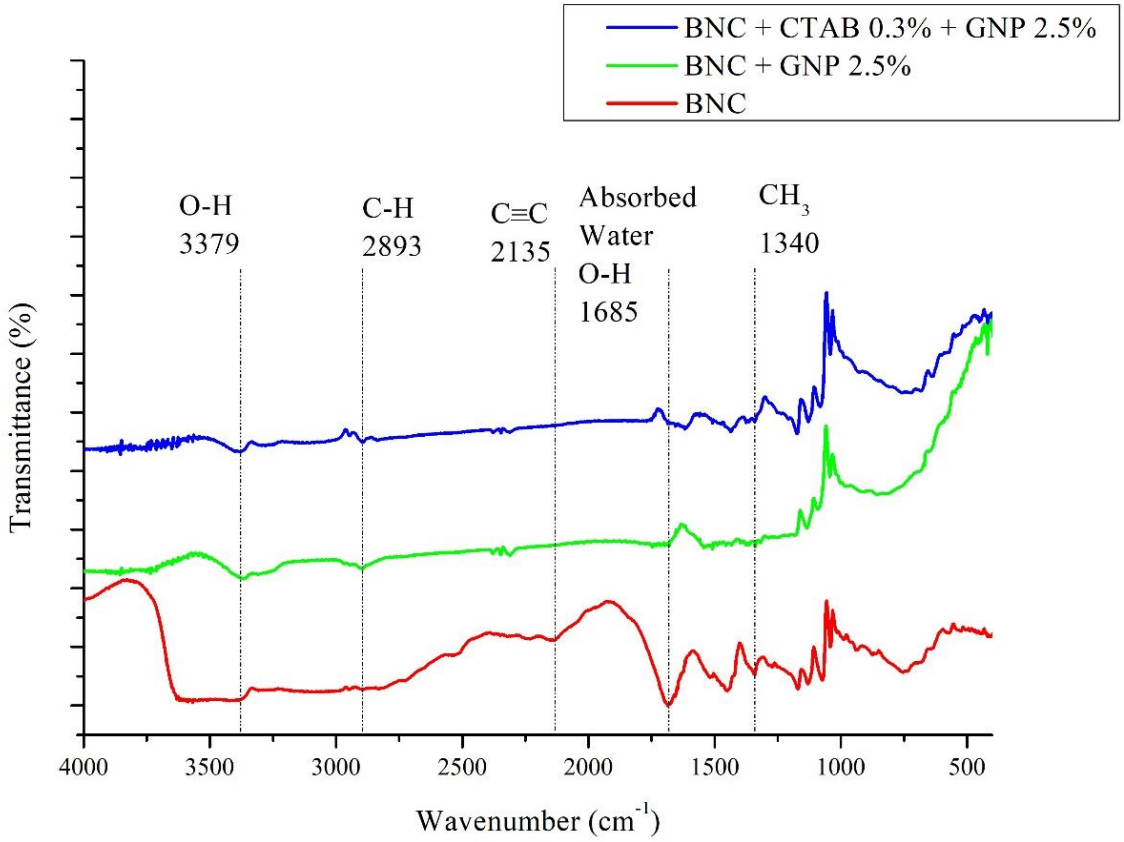

Fig. 2. FTIR spectra of BNC/GNP composite films.

C. XRD Analysis

The structure of BNC/GNP composite films was analyzed using X-Ray Diffractogram presented in Fig. 3. The XRD spectra of BNC composite films show three distinct peaks, which appear at 2θ 14.2º, 18.2º, and 22.8º, corresponding to crystallographic planes of (101), (101) and (002) [18]. For BNC/GNP composite films, the XRD spectrum show one more distinct peak at 2θ 26.4º that correspond to GNP crystal (002). Crystalline index (C.I), and % of crystalline were calculated based on X-Ray Diffractogram, and the results were listed in Table 1. The C.I value of BNC film increase after penetration and interaction by GNP. This GNP agglomerates and form a bundle on the surface of BNC and does not disperse uniformly into the BNC matrix. CI value decrease in BNC/GNP composite film with CTAB

addition. The interaction of CTAB with GNP cause polar and hydrophobic properties of GNP to lower. This condition makes GNP disperse uniformly in water solvent and evenly distributed into the BNC matrix. They result in lower crystallinity for BNC/CTAB/GNP composite films.

Table 1. Crystallinity Index and % Crystalline of the composite films

No	Sample	C.I	% Crystalline
1	Control	0.565631	69.71707
2	BNC/GNP 2.5%	0.98676	98.69334
3	BNC/CTAB/GNP 2.5%	0.825846	85.16771

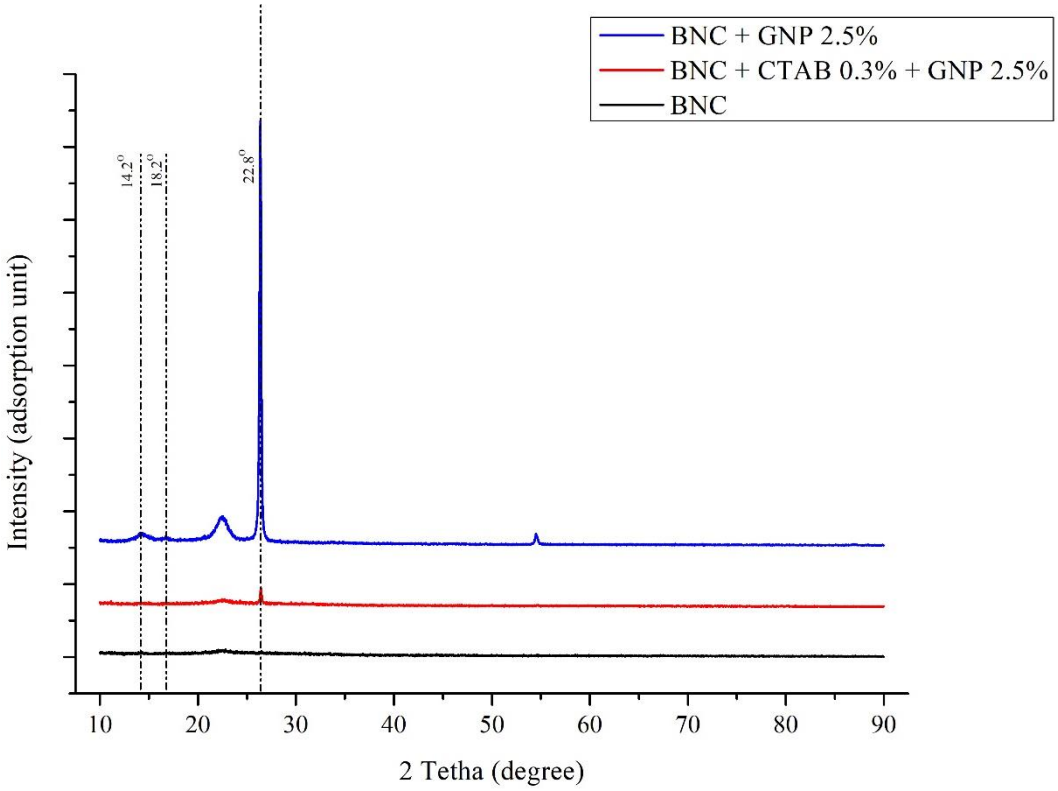

Fig. 3. X-ray diffraction spectra of BNC/GNP composite films

D. Tensile Strength Analysis

The mechanical strength of BNC/GNP composite films was analyzed from the tensile test result. Fig. 4 shows the tensile stress-strain diagrams of BNC/GNP composite films. Pure BNC films have the lowest tensile strength, about 10.4 ± 0.415. The addition of GNP as filler into BNC matrix has successfully significantly increased the mechanical strength of BNC/GNP composite film [33]. Interactions between the BNC and GNP might become crucial contributors to increasing the mechanical properties of composite film because of the existence of hydroxyl groups of BNC and the functional groups of GNP during the sonication treatment [[21]. But after the addition of CTAB into BNC/GNP composite film, the mechanical strength has become weaker. The presence of CTAB results in a lower amount of O-H bond, which is affected the mechanical properties of the composite film.

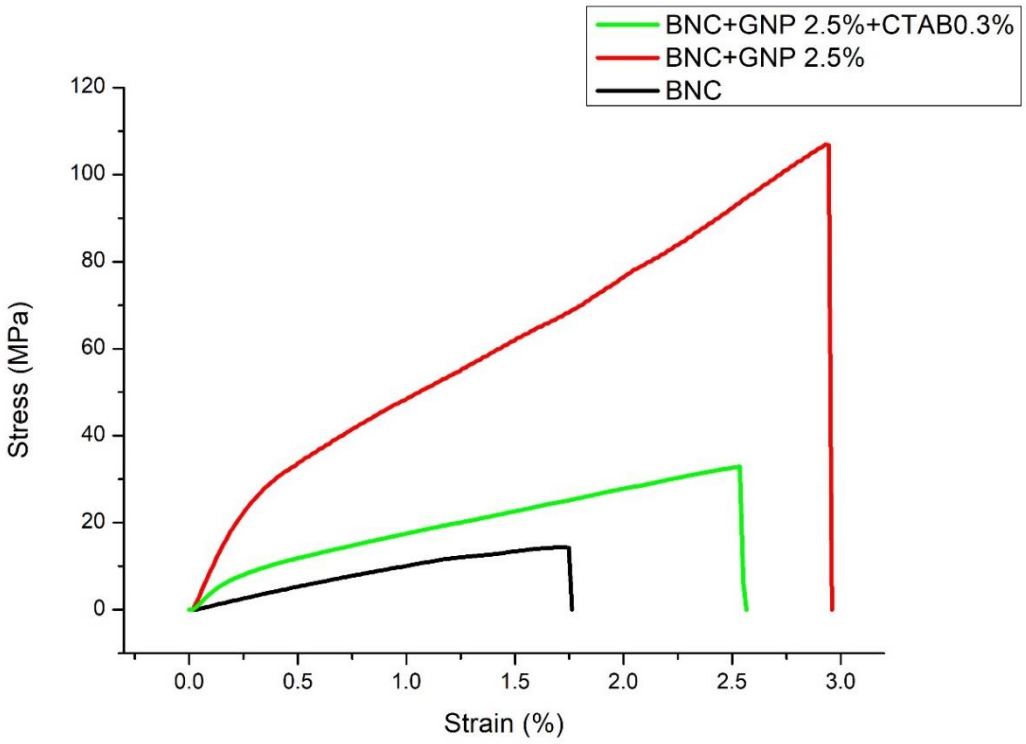

Fig. 4. Tensile stress-strain diagrams of BNC/GNP composite films.

Table 2 shows the mechanical properties of BNC/GNP composite films. The strongest tensile strength belongs to BNC/GNP composite films which the maximum stress strength reaches 103.17 ± 8.5 MPa with Young's modulus 77.01 ± 8.564. BNC/GNP composite films with CTAB addition has lower mechanical properties, and BNC film has the lowest mechanical properties with a stress strength of 13.99 ± 2.769 MPa.

Table 2. Mechanical properties of BNC./GNP composite films

Sampel	Thickness (mm)	Stress (MPa)	Strain (%)	Young's Modulus
BNC	0.04 ± 0.002	13.99 ± 2.769	1.63 ± 0.431	10.4 ± 0.415
BNC/GNP 2.5%	0.04 ± 0.001	103.17 ± 8.5	2.61 ± 0.349	77.01 ± 8.564
BNC/GNP 2.5%/CTAB	0.06 ± 0.003	34.35 ± 3.505	2.11 ± 0.469	31.14 ± 1.97

IV. Conclusions

BNC/GNP composite films with addition CTAB were successfully prepared through incorporating GNP-CTAB solution into BNC solution with sonication process and dried by an oven. CTAB addition to BNC/GNP composite changes its morphology. GNP seems evenly distributed into the BNC matrix. This also identified at C.I of BNC/CTAB/GNP composite films that are lower than BNC/GNP composite films. O-H peak stretching was detected at wavenumber 3379 $cm^{-1,}$ and it tends to decrease while the amount of GNP increase in the composite films. BNC/GNP composite films have the best mechanical

properties with Young's modulus about 77.01 ± 8.564. CTAB addition on BNC/GNP films results in lower mechanical properties.

Acknowledgment

A great appreciation was delivered to LP2M-UM through the PNBP-PUI/CAMRY research grant 2021 with contract no. 5.3.837/UN32.14.1/LT/2021

References

[1] M. P. Illa, M. Khandelwal, and C. S. Sharma, "Bacterial cellulose-derived carbon nanofibers as anode for lithium-ion batteries," *Emergent Mater.*, vol. 1, no. 3–4, pp. 105–120, 2018, doi: 10.1007/s42247-018-0012-2.

[2] A. Tayeb, E. Amini, S. Ghasemi, and M. Tajvidi, "Cellulose Nanomaterials—Binding Properties and Applications: A Review," *Molecules*, vol. 23, no. 10, p. 2684, Oct. 2018, doi: 10.3390/molecules23102684.

[3] I. de A. A. Fernandes, A. C. Pedro, V. R. Ribeiro, D. G. Bortolini, M. S. C. Ozaki, G. M. Maciel, and C. W. I. Haminiuk, "Bacterial cellulose: From production optimization to new applications," *Int. J. Biol. Macromol.*, vol. 164, pp. 2598–2611, 2020, doi: 10.1016/j.ijbiomac.2020.07.255.

[4] M. P. Illa, C. S. Sharma, and M. Khandelwal, "Catalytic graphitization of bacterial cellulose–derived carbon nanofibers for stable and enhanced anodic performance of lithium-ion batteries," *Mater. Today Chem.*, vol. 20, p. 100439, 2021, doi: 10.1016/j.mtchem.2021.100439.

[5] M. Iguchi, S. Yamanaka, and A. Budhiono, "Bacterial cellulose - a masterpiece of nature's arts," *J. Mater. Sci.*, vol. 35, no. 2, pp. 261–270, 2000, doi: 10.1023/A:1004775229149.

[6] D. Klemm, F. Kramer, S. Moritz, T. Lindström, M. Ankerfors, D. Gray, and A. Dorris, "Nanocelluloses: A new family of nature-based materials," *Angew. Chemie - Int. Ed.*, vol. 50, no. 24, pp. 5438–5466, 2011, doi: 10.1002/anie.201001273.

[7] T. A. Agustin and A. Putra, "The Effect of Addition of Polyethylene Glycol (PEG) on Biodegradable Plastic Based on Bacterial Cellulosa from Coconut Water (Coconus Nucifera)," *Int. J. Progress. Sci. Technol.*, vol. 17, no. 2, pp. 50–57, 2019, doi: 10.52155/ijpsat.v17.2.1398.

[8] H. Suryanto, T. A. Sutrisno, U. Yanuhar, and R. Wulandari, "Morphology and structure of bacterial cellulose film after ionic liquid treatment," *J. Phys. Conf. Ser.*, vol. 1595, no. 1, p. 012028, Jul. 2020, doi: 10.1088/1742-6596/1595/1/012028.

[9] J. Gutierrez, A. Tercjak, I. Algar, A. Retegi, and I. Mondragon, "Conductive properties of TiO 2/bacterial cellulose hybrid fibres," *J. Colloid Interface Sci.*, vol. 377, no. 1, pp. 88–93, 2012, doi: 10.1016/j.jcis.2012.03.075.

[10] S. A. Sardjono, H. Suryanto, Aminnudin, and M. Muhajir, "Crystallinity and morphology of the bacterial nanocellulose membrane extracted from pineapple peel waste using high-pressure homogenizer," *AIP Conf. Proc.*, vol. 2120, 2019, doi: 10.1063/1.5115753.

[11] J. Juntaro, M. Pommet, A. Mantalaris, M. Shaffer, and A. Bismarck, "Nanocellulose enhanced interfaces in truly green unidirectional fibre reinforced composites," *Compos. Interfaces*, vol. 14, no. 7–9, pp. 753–762, 2007.

[12] S. Dutta, J. Kim, Y. Ide, J. H. Kim, M. S. A. Hossain, Y. Bando, Y. Yamauchi, and K. C.-W. Wu, "3D network of cellulose-based energy storage devices and related emerging applications," *Mater. Horizons*, vol. 4, no. 4, pp. 522–545, 2017.

[13] R. Sabo, A. Yermakov, C. T. Law, and R. Elhajjar, "Nanocellulose-enabled electronics, energy harvesting devices, smart materials and sensors: A review," *J. Renew. Mater.*, vol. 4, no. 5, pp. 297–312, 2016.

[14] R. Wulandari, H. F. Aritonang, and A. D. Wuntu, "Sintesis Dan Karakterisasi Nanografit," *Chem. Prog.*, vol. 10, no. 2, pp. 46–49, 2017, doi: 10.35799/cp.10.2.2017.27745.

[15] H. F. Aritonang, R. Wulandari, and A. D. Wuntu, "Synthesis and Characterization of Bacterial Cellulose/Nano-Graphite Nanocomposite Membranes," *Macromol. Symp.*, vol. 391, no. 1, p. 1900145, Jun. 2020, doi: 10.1002/masy.201900145.

[16] Y. Li, Z. Sun, D. Liu, S. Lu, F. Li, G. Gao, M. Zhu, M. Li, Y. Zhang, H. Bu, Z. Jia, and S. Ding, "Bacterial Cellulose Composite Solid Polymer Electrolyte With High Tensile Strength and Lithium Dendrite Inhibition for Long Life Battery," *ENERGY Environ. Mater.*, p. eem2.12122, Oct. 2020, doi: 10.1002/eem2.12122.

[17] R. Metz, C. Blanc, S. Dominguez, S. Tahir, R. Leparc, and M. Hassanzadeh, "Nonlinear field dependent conductivity dielectrics made of graphite nanoplatelets filled composites," *Mater. Lett.*, vol. 292, p. 129611, 2021.

[18] E. Erbas Kiziltas, A. Kiziltas, K. Rhodes, N. W. Emanetoglu, M. Blumentritt, and D. J. Gardner, "Electrically conductive nano graphite-filled bacterial cellulose composites," *Carbohydr. Polym.*, vol. 136, pp. 1144–1151, Jan. 2016, doi: 10.1016/j.carbpol.2015.10.004.

[19] Y. M. Shulga, A. V. Melezhik, E. N. Kabachkov, F. O. Milovich, N. V. Lyskov, A. V. Irzhak, N. N. Dremova, G. L. Gutsev, A. Michtchenko, A. G. Tkachev, and Y. Kumar, "Characterisation and electrical conductivity of polytetrafluoroethylene/graphite nanoplatelets composite films," *Appl. Phys. A Mater. Sci. Process.*, vol. 125, no. 7, pp. 1–8, 2019, doi:10.1007/s00339-019-2747-x.

[20] X. Wei, X. zheng Jin, N. Zhang, X. dong Qi, J. hui Yang, Z. wan Zhou, and Y. Wang, "Constructing cellulose nanocrystal/graphene nanoplatelet networks in phase change materials toward intelligent thermal management," *Carbohydr. Polym.*, vol. 253, no. August 2020, p. 117290, 2021, doi: 10.1016/j.carbpol.2020.117290.

[21] G. Li, X. Tian, X. Xu, C. Zhou, J. Wu, Q. Li, L. Zhang, F. Yang, and Y. Li, "Fabrication of robust and highly thermally conductive nanofibrillated cellulose/graphite nanoplatelets composite papers," *Compos. Sci. Technol.*, vol. 138, pp. 179–185, 2017, doi: 10.1016/j.compscitech.2016.12.001.

[22] O. S. Yakovenko, L. Y. Matzui, L. L. Vovchenko, O. V. Lozitsky, O. I. Prokopov, O. A. Lazarenko, A. V. Zhuravkov, V. V. Oliynyk, V. L. Launets, S. V. Trukhanov, and A. V. Trukhanov, "Electrophysical properties of epoxy-based composites with graphite nanoplatelets and magnetically aligned magnetite," *Mol. Cryst. Liq. Cryst.*, vol. 661, no. 1, pp. 68–80, Jan. 2018, doi: 10.1080/15421406.2018.1460243.

[23] B. Li and W.-H. Zhong, "Review on polymer/graphite nanoplatelet nanocomposites," *J. Mater. Sci.*, vol. 46, no. 17, pp. 5595–5614, Sep. 2011, doi: 10.1007/s10853-011-5572-y.

[24] H. Suryanto, T. A. Sutrisno, M. Muhajir, N. Zakia, and U. Yanuhar, "Effect of peroxide treatment on the structure and transparency of bacterial cellulose film," in *MATEC Web of Conferences*, 2018, vol. 204, p. 5015.

[25] S. A. Sardjono, H. Suryanto, Aminnudin, and M. Muhajir, "Crystallinity and morphology of the bacterial nanocellulose membrane extracted from pineapple peel waste using high-pressure homogenizer," in *AIP Conference Proceedings*, Jul. 2019, vol. 2120, p. 080015. doi: 10.1063/1.5115753.

[26] E. Serag, A. El Nemr, and A. El-Maghraby, "Synthesis of highly effective novel graphene oxide-polyethylene glycol-polyvinyl alcohol nanocomposite hydrogel for copper removal," *J. Water Environ. Nanotechnol.*, vol. 2, no. 4, pp. 223–234, 2017.

[27] L. Segal, J. J. Creely, A. E. Martin Jr, and C. M. Conrad, "An empirical method for estimating the degree of crystallinity of native cellulose using the X-ray diffractometer," *Text. Res. J.*, vol. 29, no. 10, pp. 786–794, 1959.

[28] ASTM D638-14, "Standard Practice for Preparation of Metallographic Specimens," *ASTM Int.*, vol. 82, no. C, pp. 1–15, 2016, doi: 10.1520/D0638-14.1.

[29] H. Suryanto, M. Muhajir, T. A. Sutrisno, U. Yanuhar, and R. D. Bintara, "Effect of Disintegration Process on the Properties of Bacterial Cellulose Foam," *Key Eng. Mater.*, vol. 851, pp. 86–91, Jul. 2020, doi: 10.4028/www.scientific.net/KEM.851.86.

[30] T. Zhou, D. Chen, J. Jiu, T. T. Nge, T. Sugahara, S. Nagao, H. Koga, M. Nogi, K. Suganuma, X. Wang, X. Liu, P. Cheng, T. Wang, and D. Xiong, "Electrically conductive bacterial cellulose composite membranes produced by the incorporation of graphite nanoplatelets in pristine bacterial cellulose membranes," *Express Polym. Lett.*, vol. 7, no. 9, pp. 756–766, 2013, doi: 10.3144/expresspolymlett.2013.73.

[31] L. Zhang, J. Zhu, W. Zhou, J. Wang, and Y. Wang, "Thermal and electrical conductivity enhancement of graphite nanoplatelets on form-stable polyethylene glycol/polymethyl methacrylate composite phase change materials," *Energy*, vol. 39, no. 1, pp. 294–302, 2012, doi: 10.1016/j.energy.2012.01.011.

[32] P. Rani, K. S. Kumar, A. D. Pathak, and C. S. Sharma, "Pyrolyzed pencil graphite coated cellulose paper as an interlayer: An effective approach for high-performance lithium-sulfur battery," *Appl. Surf. Sci.*, vol. 533, no. August, p. 147483, Dec. 2020, doi: 10.1016/j.apsusc.2020.147483.

[33] F. Wang and L. T. Drzal, "The use of cellulose nanofibrils to enhance the mechanical properties of graphene nanoplatelets papers with high electrical conductivity," *Ind. Crops Prod.*, vol. 124, no. August, pp. 519–529, 2018, doi: 10.1016/j.indcrop.2018.08.019.